Journal of Power Sources 196 (2011) 928–934

Contents lists available at ScienceDirect

Journal of Power Sources

journal homepage: www.elsevier.com/locate/jpowsour

Performance of (La,Sr)MnO_3 cathode based solid oxide fuel cells: Effect of bismuth oxide sintering aid in silver paste cathode current collector

Yunhui Gong, Weijie Ji, Lei Zhang, Bin Xie, Haiqian Wang*

Hefei National Laboratory for Physical Sciences at the Microscale, and USTC-Shincron Joint Lab, University of Science and Technology of China (USTC), Hefei 230026, PR China

ARTICLE INFO

Article history:
Received 30 June 2010
Received in revised form 30 August 2010
Accepted 31 August 2010
Available online 6 September 2010

Keywords:
Solid oxide fuel cell
Bismuth oxide
Silver paste current collector
Electrochemical performance

ABSTRACT

Effects of a bismuth oxide (Bi_2O_3) sintering aid in the silver paste cathode current collectors on the electrochemical performance of solid oxide fuel cells with (La,Sr)MnO_3 cathode is investigated. Anode-supported single cells are prepared and applied with pure and Bi_2O_3-added silver pastes for cathode current collecting. Cell performances are evaluated using a current–voltage test and electrochemical impedance spectroscopy. The results indicate that the Bi_2O_3-added silver paste cathode current collector artificially increases the power density and lowers the polarization resistance of single cell, which may be attributed to the observation of the improved cathode current collector surface morphology and enhanced contact at the cathode-current collector interface, as well as the migration of the Bi_2O_3 and silver into the cathode from the Bi_2O_3 contained silver paste cathode current collector.

1. Introduction

A solid oxide fuel cell (SOFC) is an electrochemical device operated at high temperature (600–1000 °C). It transforms the chemical energy stored in fuels into electrical energy and heat [1–3]. A solid oxide fuel cell (SOFC) is composed of an anode and cathode separated by an electrolyte membrane [4,5]. Yttria-stabilized zirconia (YSZ) is the most widely used oxygen-ion conducting ceramic electrolyte, meanwhile nickel–YSZ composite and strontium doped lanthanum manganite (LSM) perovskites are commonly employed as the anode and cathode materials, respectively [6–10]. The electrochemical performance of a SOFC depends on not only the internal resistance of the positive-electrolyte-negative (PEN) structure, but also on the electrical contacts across the electrodes to the external circuit. In a laboratory-scale test, electrical current collectors formed by noble metals, such as platinum or silver, are often applied on top of electrodes to minimize contact resistance [11–28].

In many studies, silver in the forms of paste, mesh and contact pins, has been selected as the cathode current collectors at operation temperatures less than 800 °C [11,13,15,18–25,27,28]. Although the mesh and contact pins are close to the practical current collector in SOFC stacks, commercial silver paste is much more convenient for academic research. Because it can be easily printed and fired to obtain good adherence to the electrodes, and the effective area can be identified accurately [13]. A low concentration of Bi_2O_3 (less than 5 wt.%) is commonly used in commercial silver paste as an inorganic sintering aid, which plays an important role in improving the surface morphology of the silver layer and increasing adhesion between the silver layer and substrate [29].

It has been reported that the electrochemical performance of electrodes is sensitive to the physical and chemical nature of the current collectors [13,20,21,28]. Therefore, it may be expected that single cells with Bi_2O_3-added and pure silver paste current collectors will exhibit different electrochemical performances. Bi_2O_3 in the silver paste may be beneficial to current collection by suppressing the current constriction effect between the cathode and current collector due to the following reasons [18]: (1) Bi_2O_3 helps form a uniform surface morphology of silver current collector [29], and (2) Bi_2O_3 reacts with LSM to create extra conductive solid solution contacts at the cathode-current collector interface [30]. In addition to this mechanism, there is also evidence indicating that Bi_2O_3 may enhance the electrochemical activity of the cathode. Bi_2O_3 has a low melting temperature of 823 °C, so migration of Bi_2O_3 may occur at the testing temperature of the SOFC [31]. As a result, some of the Bi_2O_3 may penetrate into the cathode. Because Bi_2O_3 has a much higher oxygen ionic conductivity than YSZ [32], the additional contacts between Bi_2O_3 and LSM in the cathode may increase the three-phase boundaries and accelerate the oxygen reduction rate. When reaching the cathode–electrolyte interface, Bi_2O_3 may improve the cathode–electrolyte interface by reducing interfacial resistance [33]. Moreover, Bi_2O_3 lowers the sintering temperature of silver phase and enhances its mass transport [29]. Migration of silver into the cathode may occur in the long-term test [20]. The condensed, highly conductive silver particles

* Corresponding author at: Hefei National Laboratory for Physical Sciences at the Microscale, University of Science and Technology of China, 96 Jinzhai Road, Hefei, Anhui 230026, China. Tel.: +86 551 3603770; fax: +86 551 3606266.
E-mail address: hqwang@ustc.edu.cn (H. Wang).

0378-7753/$ – see front matter © 2010 Elsevier B.V. All rights reserved.
doi:10.1016/j.jpowsour.2010.08.104

are known to improve the electron supply for oxygen exchange reactions [34].

In the present study, LSM-based anode-supported SOFCs were fabricated. Pure and Bi_2O_3-added silver pastes were applied to single cells for cathode current collecting, respectively. Cells tested under the same conditions were observed to exhibit variable electrochemical performances. Possible mechanisms are proposed and discussed to understand the effect of the Bi_2O_3 additive in the silver paste. However, the purpose of this paper is not to suggest an approach for improving cell performance, but rather to present an artifact of the measurement technique that originated from using Bi_2O_3-added silver paste as a cathode current collector.

2. Experimental

2.1. Preparation of anode-supported fuel cells

The anode was comprised of a porous supporting substrate and a thin, less porous functional layer. The substrate was composed of coarse NiO (Sinopharm Chemical Reagent, China) and YSZ (BQ-8Y, Jiaozuo Weina Fine Ceramic, China) in a ratio of 55 and 45 wt.% and was produced using a tape-casting process. The functional layer was deposited using a suspension spray method with fine NiO (J.T. Baker, USA) and YSZ (TZ-8Y, Tosoh, Japan) in the same weight ratio. The green layer was co-sintered in air at 1400 °C for 5 h. The resulting porous substrate and functional layer were 500 and 15 μm thick, respectively.

A 9 mol.% YSZ film was deposited on the smooth anode from a metallic Zr–Y target (92:8 wt.%) in a mid frequency reactive magnetron sputtering system (ASC-800, Shincron Co. Ltd., Japan) [35]. A 35 mm × 35 mm anode was used. The base vacuum level was below 2×10^{-4} Pa. During the deposition, the total pressure was 0.17 Pa, and the flow rates of argon and oxygen were 50 and 150 sccm, respectively. The sputtering power was kept at 3 kW, and the deposition rate was 0.5 μm h^{-1}. The as-prepared YSZ film was annealed in air at 1200 °C for 4 h to obtain a dense electrolyte.

The cathode consisted of a functional layer (CFL) and a current collecting layer (CCCL) with an active surface area of 20 mm × 20 mm. The CFL was deposited by screen printing a mixture of 50 wt.% $(La_{0.8}Sr_{0.2})_{0.95}MnO_3$ (Nextech, USA) and 50 wt.% YSZ (TZ-8Y, Tosoh, Japan) on top of the electrolyte. The CCCL was then screen printed onto the CFL layer. Finally, the cells were co-sintered in air at 1150 °C for 3 h. The thickness of CFL and CCCL were about 8 and 30 μm, respectively.

2.2. Application of silver pastes

Three types of silver pastes, denoted as 0Bi–Ag, 2Bi–Ag and 3Bi–Ag, were applied to the cathodes as current collectors. 0Bi–Ag paste was made from pure silver powder (Gold and Silver Refinery of CBPMC, China). 2Bi–Ag was composed of the same silver and 2 wt.% Bi_2O_3 powder (Sinopharm Chemical Reagent Co. Ltd., China). The solid powders were mixed with a terpineol-ethylcellulose vehicle in a weight ratio of 7:3 and milled in an agate mortar. 3Bi–Ag paste is a commercial silver paste with 3 wt.% Bi_2O_3, as determined by an inductively coupled plasma atomic emission spectrometer (ICP-AES) (Atomscan Advantage, Jarrell Ash, USA). These pastes were screen printed on the cathode using a 200 API stainless steel mesh and were subsequently sintered at 800 °C for 30 min. The average thickness of the silver paste current collectors was about 10 μm.

2.3. Characterization of silver paste current collector

A nano-scratch test [36] was conducted using a nanoindenter instrument (Hysitron TriboIndenter) to evaluate adhesion between the LSM cathode and different silver paste current collectors. During the test, a diamond indenter tip was used to draw along the surface of the silver paste current collector. A compressive stress was induced ahead of the indenter. An increasing normal load was applied to the indenter until the radial compressive stress reached a critical value to delaminate the current collector from the cathode. The measured critical load is used to describe the adhesive force. The testing silver paste current collectors were prepared with a 400 API stainless steel mesh to keep the thickness under the range of the instrument. Five scratches on each sample surface were studied in the progressive normal force mode.

Sheet resistances of the silver current collectors on commercial 96% alumina substrates were measured with a Keithley sourcemeter (2420-C) using the four-probe method and were calculated as RWL^{-1} (R is the measured resistance, W is the width of the film and L is the length in the direction of resistance measurement).

2.4. Fuel cell test and microstructure characterization

Electrochemical measurements were performed with a four-probe method. Single cells were sealed to stainless steel holders using silver conductive adhesive (DAD87, Shanghai Research Institute of Synthetic Resins, China). The silver sealant also served for anode current collecting. Afterwards, silver mesh was pressed onto the silver paste cathode current collector. Silver wire leads were attached to both the anode and cathode with silver adhesive. The test apparatus was slowly heated and fed with 30 sccm N_2. After the temperature was brought to 800 °C, NiO was reduced to Ni by a stepwise replacement of N_2 with H_2. The electrochemical performances of single cells were measured between 700 and 800 °C. The flow rates of humidified H_2 (bubbled through water at room temperature) and air were 300 and 1200 sccm in the test, respectively. The current–voltage data were acquired using an electronic load (6060B, Agilent). The impedance was measured using an electrochemical station (IM6EX, Zahner) in the frequency range of 0.05–10^5 Hz with AC amplitude of 20 mV at open circuit voltage (OCV). The tested cells were analyzed by scanning electron microscopy (SEM, JSM-6700, JEOL) and energy-dispersive X-ray spectroscopy (EDX, INCA, Oxford instrument). The surface morphologies of the silver paste current collectors on LSM were investigated in the lower second electron image (LEI) mode. The cross sectional microstructures of fractured samples were examined in the backscattered electron (BSE) modes. The chemical stability of the cathode was characterized by X-ray diffraction (XRD, X'Pert PRO, PHILIPS) using Cu Kα radiation. To verify the possible reaction between Bi_2O_3 and the sputtered YSZ electrolyte, a thin layer of Bi_2O_3 was screen printed on top of the electrolyte and heated to 800 °C. Microstructures of the sputtered YSZ electrolyte before and after the reaction were characterized with SEM.

3. Results

3.1. Electrochemical performances of single cells

Fig. 1 shows the I–V and I–P curves of cells with different silver paste current collectors at 800, 750 and 700 °C with humidified hydrogen as the fuel and air as the oxidant. The observed open circuit voltages are higher than 1.05 V, indicating that the YSZ electrolyte is dense and gas-tight. The power densities of single cells at 0.7 V and different testing temperatures are summarized in Table 1. Clearly, the power outputs of the cells are enhanced by increasing the Bi_2O_3 content in silver pastes. Because the cells were fabricated and tested under the same conditions, variation in their performances can be mainly ascribed to the different silver pastes.

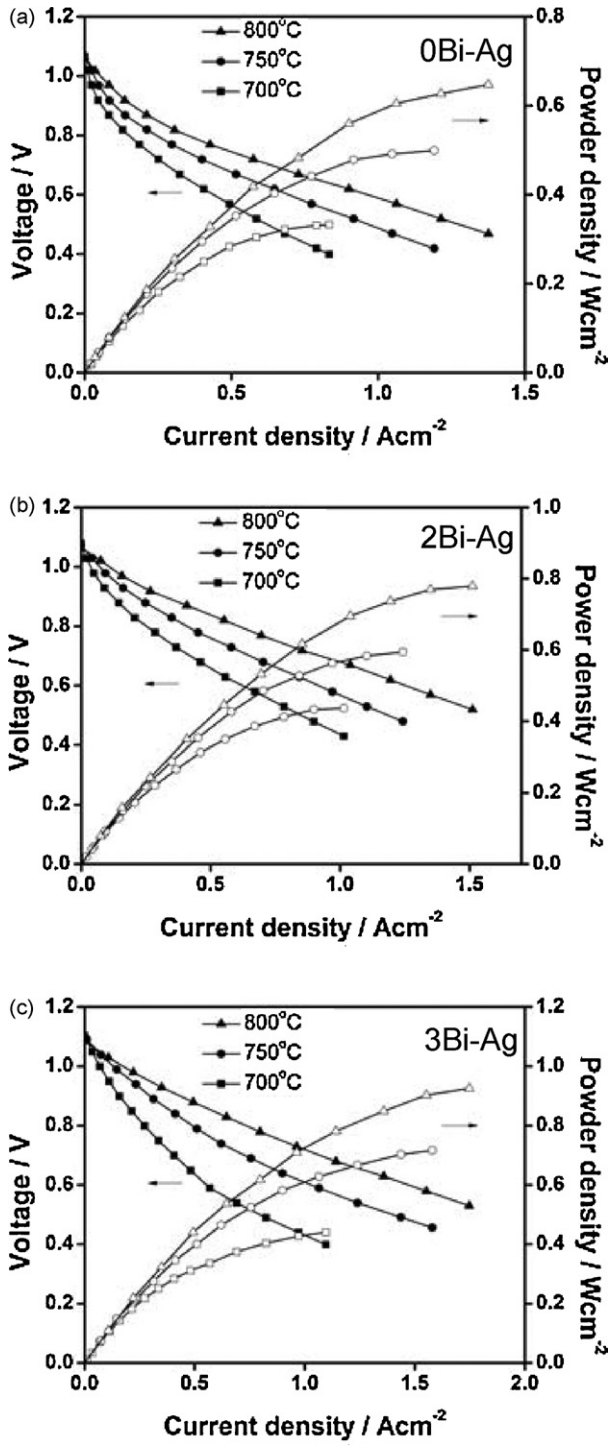

Fig. 1. Current–voltage measurements of single cells with different silver paste current collectors tested from 700 to 800 °C: (a) 0Bi–Ag paste, (b) 2Bi–Ag paste, and (c) 3Bi–Ag paste.

Table 1
Power densities (at 0.7 V) of SOFCs with different silver paste current collectors.

Temperature (°C)	Power density at 0.7 V (W cm^{-2})		
	0Bi–Ag paste	2Bi–Ag paste	3Bi–Ag paste
800	446	649	748
750	312	458	513
700	194	285	294

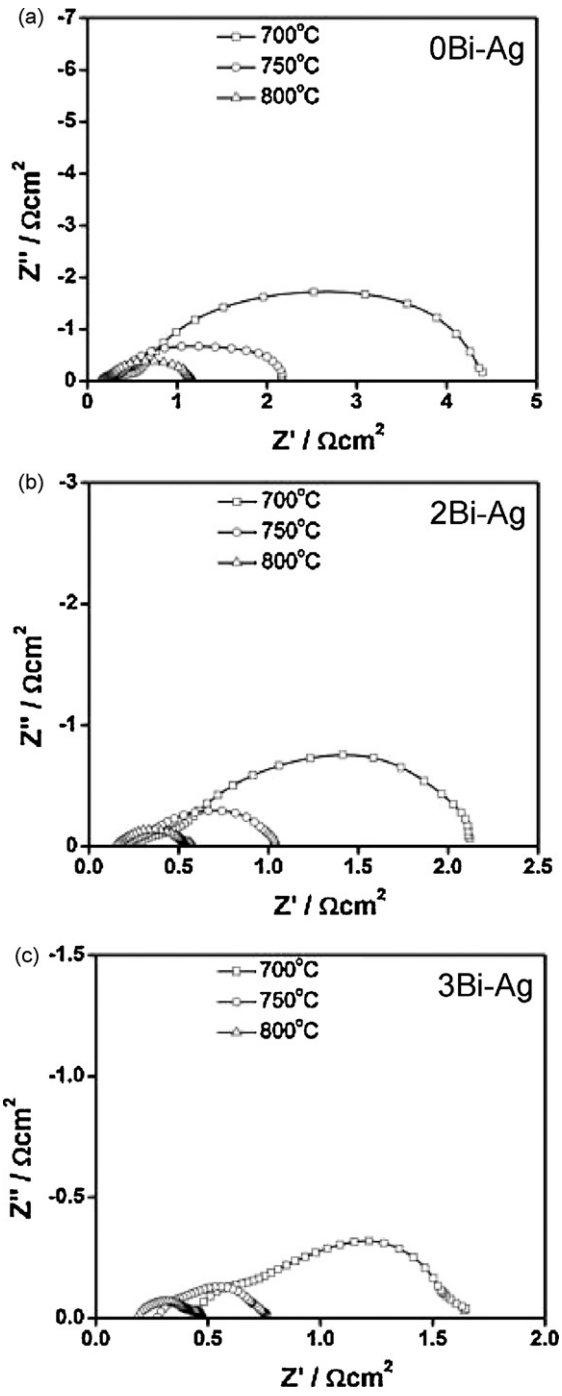

Fig. 2. AC impedance spectroscopy of single cells with different silver paste current collectors at OCV: (a) 0Bi–Ag paste, (b) 2Bi–Ag paste, and (c) 3Bi–Ag paste.

Fig. 2 shows the ac impedance spectra of cells with different silver paste current collectors measured from 0.05 to 10^5 Hz under the open circuit condition. The low- and high-frequency real-axis intercepts correspond to the total resistance (R_{total}) and ohmic resistance (R_{ohm}), respectively. The difference between the low- and high-frequency intercepts on the real axis can be interpreted as the polarization resistance (R_{pol}) [37]. The measured results of R_{total}, R_{ohm} and R_{pol} are listed in Table 2. It can be seen that R_{total} and R_{pol} decrease as the Bi_2O_3 content increases in the silver pastes, whereas R_{ohm} exhibits the opposite trend. In addition, our results show that the measured R_{pol}, mainly from the contribution of the cathode process [12], accounts for at least 60% of the total resis-

Table 2
Area specific resistance (at OCV) of SOFCs with different silver paste current collectors.

Temperature (°C)	Specific area resistance (Ω cm^2)								
	0Bi–Ag paste			2Bi–Ag paste			3Bi–Ag paste		
	R_{ohm}	R_{pol}	R_{total}	R_{ohm}	R_{pol}	R_{total}	R_{ohm}	R_{pol}	R_{total}
800	0.143	1.02	1.163	0.146	0.432	0.578	0.182	0.292	0.474
750	0.189	1.976	2.165	0.202	0.839	1.041	0.276	0.486	0.762
700	0.266	4.134	4.4	0.287	1.823	2.11	0.431	1.210	1.641

R_{total} and R_{ohm} were obtained from the low-frequency and high-frequency intercept of the AC impedance spectrum, respectively. R_{pol} was calculated from subtracting the R_{ohm} from the R_{total}.

tance. The distinct behaviors of R_{ohm} and R_{pol} are believed to be related to the different silver pastes.

3.2. Characterization of the silver paste current collectors

Fig. 3 displays the surface micrographs of the silver paste current collectors. Although the surface microstructures differ from each other, all of them present enough porosity for oxygen diffusion into the cathode. It can be seen from Fig. 3(a) that the 0Bi–Ag paste current collector has a rough surface morphology, containing large cracks and many small pores, which may decrease connection of the silver phase. By adding 2 wt.% Bi_2O_3 to the silver paste, enhanced grain growth and more uniform surface morphology can be observed in the 2Bi–Ag paste current collector, as shown in Fig. 3(b). However, a few large cracks still exist. The most improved surface morphology with uniformly distributed small pores and continuous silver grains is observed in Fig. 3(c), due to the highest content of fully dispersed Bi_2O_3 in the 3Bi–Ag paste current collector. Uniform surface morphology and less cracks have been proven to increase the conductivity of sintered silver paste current collectors, resulting in reduction of ohmic loss of the current collector [29]. Referring to Fig. 4, the measured electronic conductivity is in accordance with the observation of surface microstructures.

Adhesion between the LSM cathode and silver paste current collector was determined as critical normal force in the nano-scratch test. The measured critical normal force (listed in Table 3) represented the force needed to detach the current collector from the cathode. It can be seen that adhesion is enhanced by increasing Bi_2O_3 content in the silver pastes. Considering the formation of the LSM–Bi_2O_3 conductive solid solution at 800 °C [30], greater critical normal force may be required to neutralize the extra contacts at the cathode-current collector interface in the Bi_2O_3-added samples.

3.3. Microstructure characterization of single cells

Fig. 5 presents the cross sectional images of the tested cells with different silver paste current collectors obtained in the backscattered electron mode. Some bright spots, confirmed to be silver using EDX analysis, can be observed in the CFL of the cell with a 2Bi–Ag current collector, and more spots can be seen in the sample with a 3Bi–Ag current collector. On the other hand, no apparent silver deposition can be observed in the sample with a 0Bi–Ag current collector. Silver has been found to migrate from the silver current collector into the cathode via surface diffusion and gas transport after long-term test [20]. The observation of silver movement in the short-term test may be interpreted as enhance-

Table 3
Data of measured thickness and critical normal force for adhesion test.

Current collector	Thickness (nm)	Critical normal force (μN)
0Bi–Ag paste	427 ± 74.5	1183.6 ± 386.2
2Bi–Ag paste	381.3 ± 24.9	1967.9 ± 205.9
3Bi–Ag paste	532.2 ± 17.4	3336.8 ± 353.3

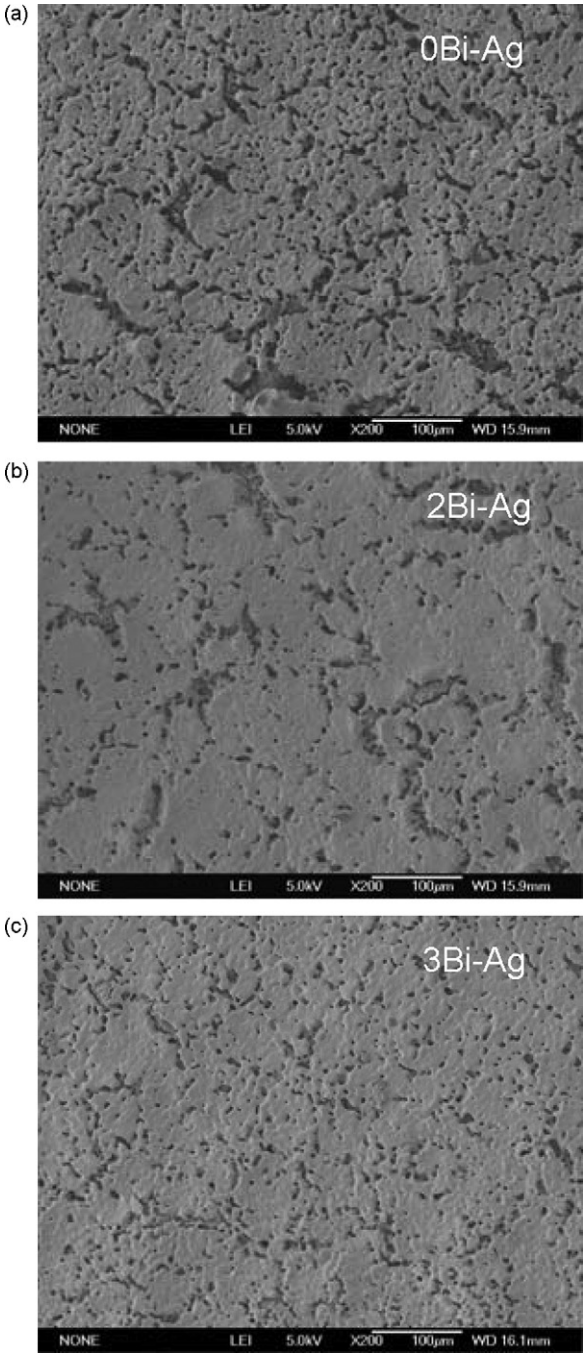

Fig. 3. Surface microstructures of different silver paste current collectors on the LSM cathode: (a) 0Bi–Ag paste, (b) 2Bi–Ag paste, and (c) 3Bi–Ag paste.

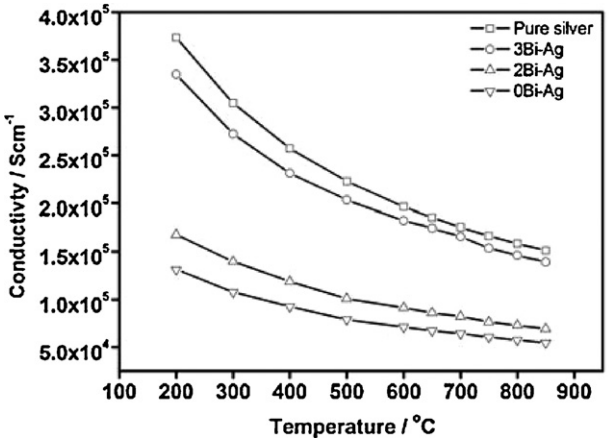

Fig. 4. Conductivities of different silver paste current collectors.

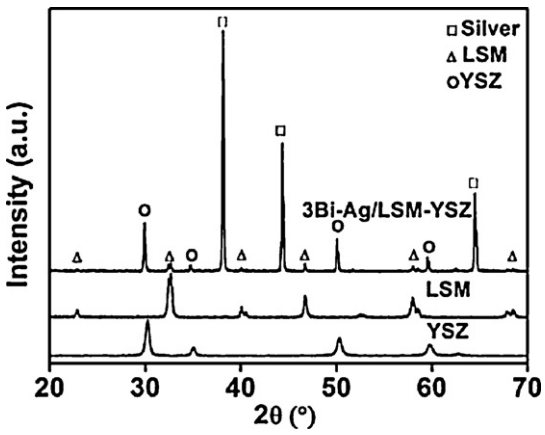

Fig. 6. XRD pattern of the LSM cathode coated with 3Bi–Ag paste.

ment of mass transfer by adding Bi_2O_3 to the silver paste. It is also notable that the ~3 μm-thick YSZ electrolyte, adjacent to the CFL (marked by white squares), changed from a bulk structure to small and irregular-shaped grains in Fig. 5(c), whereas no transformation of the electrolyte can be found in Fig. 5(a) and (b).

Fig. 6 shows the XRD pattern of the LSM cathode with a 3Bi–Ag current collector. The patterns of LSM and YSZ powders are also shown as references. Bi_2O_3 is known to cause a reaction between LSM and YSZ that forms a low conduction phase $La_2Zr_2O_7$ (LZO) at 800 °C [21]. However, the peaks reveal no evidence of LZO using the 3Bi–Ag paste current collector.

Fig. 7 displays the microstructures of the sputtered YSZ electrolyte before and after the reaction with Bi_2O_3 at 800 °C. The heating procedure was the same as that used in preparing the silver paste current collector. Obviously, the reaction causes much more severe degradation in the YSZ electrolyte than the observa-

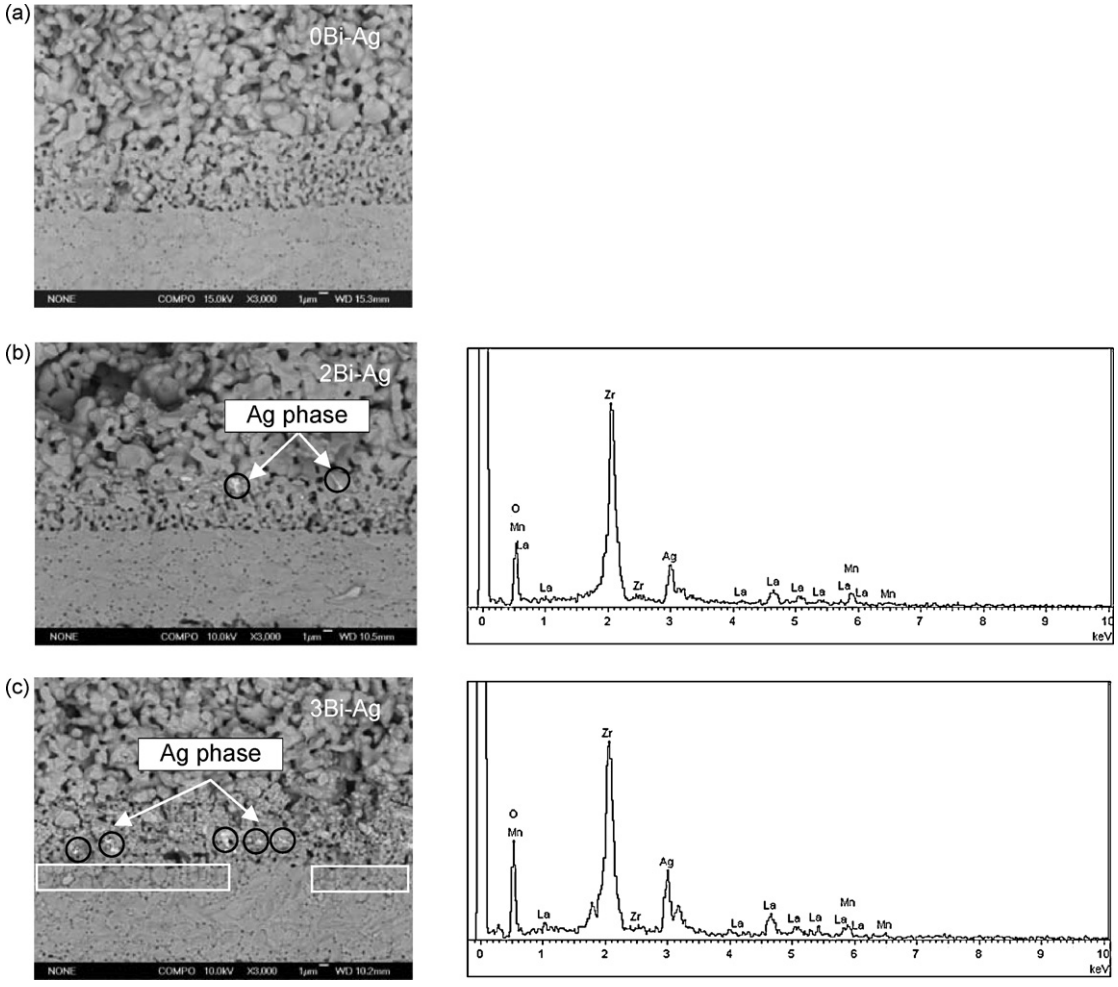

Fig. 5. Backscattered electron images of fractured single cells with different silver paste current collectors at the cathode side and EDX spectroscopy of marked areas: (a) 0Bi–Ag paste, (b) 2Bi–Ag paste and composition of marked area, and (c) 3Bi–Ag paste and composition of marked area.

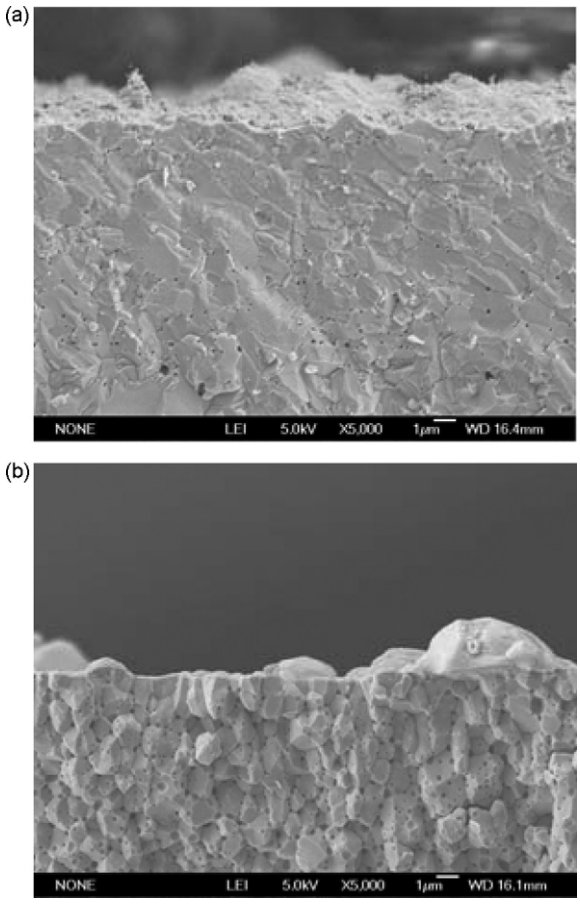

Fig. 7. Microstructures of a sputtered YSZ electrolyte before and after reacting with Bi_2O_3 and at 800 °C: (a) before reaction and (b) after reaction.

tion shown in Fig. 5(c). The entire bulk structure transformed into small grains with pores at the grain boundaries.

4. Discussion

The above results show that the Bi_2O_3 additive in the silver paste current collectors affects the electrochemical performances of single cells. According to the comparison in Table 1, the cells exhibit enhanced power output as the Bi_2O_3 content is increased in the silver paste, indicating reduction of total resistance. This is in good agreement with the result of R_{total} measured in the impedance test. The decrease of R_{pol} is dominant in R_{total}, despite the opposite trend observed for R_{ohm} (shown in Table 2).

The ohmic resistance primarily includes the electrolyte resistance, electrode ohmic resistance, and contact resistances at the interfaces of the cell components [16,26,37]. As mentioned, the Bi_2O_3-added silver paste current collectors show higher electronic conductivity and better contact to the cathode, which should lower the ohmic resistances of the current collector and at the cathode-current collector interface. Regarding the cathode, neither a difference in thickness, contact at the interfaces between the CCCL, CFL and electrolyte, nor a low conductive phase (LZO) can be found. Meanwhile, the highly electron conductive silver phase migrated from the Bi_2O_3-added silver paste current collectors can be observed in the cathode, which should reduce its ohmic resistance. Therefore, it is reasonable to assume that the increase of R_{ohm} should be induced from the resistance of the electrolyte. This can be explained by the increased grain boundaries in the YSZ electrolyte shown in Figs. 5(c) and 7(b) because the intergranular conductivity of YSZ is 2–3 orders of magnitude lower than its intragranular conductivity [38]. However, reasons for the reaction between Bi_2O_3 and the sputtered YSZ electrolyte and formation of grain boundaries are not yet clear.

To identify the origins of enhanced cell performance resulting from Bi_2O_3-added silver pastes, characteristics of the current collector were initially considered. Uniform surface morphology and increased contact to the cathode may contribute to promotion of the power outputs by suppressing current constriction at the cathode-current collector interface [18,39]. However, this is not adequate to explain the reduction of R_{pol} measured at OCV because there was no current passing through the cathode in the impedance test. The migration of Bi_2O_3 and silver into the cathode, as shown in Figs. 5(b), (c) and 7(b), seems to be responsible for the reduction of R_{pol}. Bi_2O_3 has a low melting temperature of 823 °C and exhibits high mobility at the operation temperatures of SOFC [31]. When the highly oxygen-ion-conductive Bi_2O_3 [32] moved from the silver paste current collector into the cathode, the contact between Bi_2O_3 and LSM may have created extra three-phase boundaries and accelerated the oxygen reduction rate. Once Bi_2O_3 reached the cathode–electrolyte interface, it may have improved the interface for faster oxygen ion transfer from the cathode to the electrolyte [33]. As a result, R_{pol} decreased with increasing Bi_2O_3 content. In addition, Bi_2O_3 enhanced the mass transport of the silver phase into the cathode. Silver is known to improve oxygen reduction activity [34,40,41]. Condensation of silver in the cathode may also make contribution to decrease polarization resistance and increase power outputs.

5. Conclusions

In the present study, we have demonstrated that the electrochemical performance of LSM-based anode-supported SOFCs was sensitive to Bi_2O_3 in their silver paste current collectors. Using a Bi_2O_3-added silver paste cathode current collector can artificially enhance the power output and reduce the polarization resistance of the SOFC. Bi_2O_3 additive may improve the surface morphology of silver paste current collector and increase contact at the cathode-current collector interface, which can suppress the current constriction effect. In addition, migration of Bi_2O_3 and silver phase into the cathode from the current collector can accelerate the oxygen reduction rate. It was also notable that the reaction between Bi_2O_3 and the sputtered YSZ electrolyte led to the formation of grain boundaries and increased the electrolyte resistance. This study suggests that it is important to pay attention to the silver paste selected for cathode current collecting to measure the real electrochemical performance without any contribution from the current collector to electrode reaction.

Acknowledgement

This work was partially supported by National Natural Science Foundation of China (Grant No. 52772109).

References

[1] N.Q. Minh, J. Am. Ceram. Soc. 76 (1993) 563–588.
[2] E. Ivers-Tiffee, A. Weber, D. Herbstritt, J. Eur. Ceram. Soc. 21 (2001) 1805–1811.
[3] S.C. Singhal, Solid State Ionics 152 (2002) 405–410.
[4] P. Singh, N.Q. Minh, Int. J. Appl. Ceram. Technol. 1 (2004) 5–15.
[5] J. Will, A. Mitterdorfer, C. Kleinlogel, D. Perednis, L.J. Gauckler, Solid State Ionics 131 (2000) 79–96.
[6] N.Q. Minh, Solid State Ionics 174 (2004) 271–277.
[7] K.C. Wincewicz, J.S. Cooper, J. Power Sources 140 (2005) 280–296.
[8] J.B. Goodenough, Ann. Rev. Mater. Res. 33 (2003) 91–128.
[9] S.P. Jiang, J. Power Sources 124 (2003) 390–402.
[10] S.P. Jiang, S.H. Chan, J. Mater. Sci. 39 (2004) 4405–4439.
[11] T. Tsai, S.A. Barnett, Solid State Ionics 93 (1997) 207–217.
[12] S. deSouza, S.J. Visco, L.C. DeJonghe, Solid State Ionics 98 (1997) 57–61.
[13] M. Guillodo, P. Vernoux, J. Fouletier, Solid State Ionics 127 (2000) 99–107.

[14] J.D. Kim, G.D. Kim, J.W. Moon, Y.I. Park, W.H. Lee, K. Kobayashi, M. Nagai, C.E. Kim, Solid State Ionics 143 (2001) 379–389.
[15] W.A. Meulenberg, O. Teller, U. Flesch, H.P. Buchkremer, D. Stover, J. Mater. Sci. 36 (2001) 3189–3195.
[16] M.J. Jorgensen, M. Mogensen, J. Electrochem. Soc. 148 (2001) A433–A442.
[17] C.R. Xia, W. Rauch, W. Wellborn, M.L. Liu, Electrochem. Solid-State Lett. 5 (2002) A217–A220.
[18] S.P. Jiang, J.G. Love, L. Apateanu, Solid State Ionics 160 (2003) 15–26.
[19] Z.P. Shao, S.M. Haile, Nature 431 (2004) 170–173.
[20] S.P. Simner, M.D. Anderson, L.R. Pederson, J.W. Stevenson, J. Electrochem. Soc. 152 (2005) A1851–A1859.
[21] C. Chervin, R.S. Glass, S.M. Kauzlarich, Solid State Ionics 176 (2005) 17–23.
[22] Y.Y. Huang, J.M. Vohs, R.J. Gorte, J. Electrochem. Soc. 152 (2005) A1347–A1353.
[23] Z.W. Wang, M.J. Cheng, Y.L. Dong, M. Zhang, H.M. Zhang, Solid State Ionics 176 (2005) 2555–2561.
[24] F. Zhao, A.V. Virkar, J. Power Sources 141 (2005) 79–95.
[25] T. Suzuki, M. Awano, P. Jasinski, V. Petrovsky, H.U. Anderson, Solid State Ionics 177 (2006) 2071–2074.
[26] K.J. Yoon, P. Zink, S. Gopalan, U.B. Pal, J. Power Sources 172 (2007) 39–49.
[27] T. Yamaguchi, S. Shimizu, T. Suzuki, Y. Fujishiro, M. Awano, J. Electrochem. Soc. 155 (2008) B423–B426.
[28] J.H. Kim, R.H. Song, D.Y. Chung, S.H. Hyun, D.R. Shin, J. Power Sources 188 (2009) 447–452.
[29] S.B. Rane, T. Seth, G.J. Phatak, D.P. Amalnerkar, M. Ghatpande, J. Mater. Sci. Mater. Electron. 15 (2004) 103–106.
[30] A. Chakraborty, H.S. Maiti, Ceram. Int. 25 (1999) 115–123.
[31] V.V. Kharton, F.M.B. Marques, A. Atkinson, Solid State Ionics 174 (2004) 135–149.
[32] P. Shuk, H.D. Wiemhofer, U. Guth, W. Gopel, M. Greenblatt, Solid State Ionics 89 (1996) 179–196.
[33] T. Tsai, S.A. Barnett, Solid State Ionics 98 (1997) 191–196.
[34] S.R. Wang, T. Kato, S. Nagata, T. Honda, T. Kaneko, N. Iwashita, M. Dokiya, Solid State Ionics 146 (2002) 203–210.
[35] H. Wang, W. Ji, L. Zhang, Y. Gong, B. Xie, Y. Jiang, Y. Song, Solid State Ionics, in press, doi:10.1016/j.ssi.2010.05.022.
[36] N. Frey, P. Mettraux, G. Zambelli, D. Landolt, Surf. Coat. Technol. 63 (1994) 167–172.
[37] Y.J. Leng, S.H. Chan, K.A. Khor, S.P. Jiang, Int. J. Hydrogen Energy 29 (2004) 1025–1033.
[38] S.Q. Hui, J. Roller, S. Yick, X. Zhang, C. Deces-Petit, Y.S. Xie, R. Maric, D. Ghosh, J. Power Sources 172 (2007) 493–502.
[39] K. Sasaki, J.P. Wurth, R. Gschwend, M. Godickemeier, L.J. Gauckler, J. Electrochem. Soc. 143 (1996) 530–543.
[40] V.A.C. Haanappel, D. Rutenbeck, A. Mai, S. Uhlenbruck, D. Sebold, H. Wesemeyer, B. Rowekamp, C. Tropartz, F. Tietz, J. Power Sources 130 (2004) 119–128.
[41] M. Camaratta, E. Wachsman, Solid State Ionics 178 (2007) 1242–1247.